Enhanced Barrier Performance of Engineered Paper by Atomic Layer Deposited Al_2O_3 Thin Films

Mirvakili, Mehr Negar; Bui, V.H.; Van Ommen, J. Ruud; Hatzikiriakos, Savvas G.; Englezos, Peter

DOI
10.1021/acsami.6b02292

Publication date
2016

Document Version
Accepted author manuscript

Published in
ACS Applied Materials and Interfaces

Enhanced Barrier Performance of Engineered Paper by Atomic Layer Deposited Al_2O_3 Thin Films

Mehr Negar Mirvakili†, Hao Van Bui‡, J. Ruud van Ommen‡, Savvas G. Hatzikiriakos†, Peter Englezos†*

† *Department of Chemical and Biological Engineering, University of British Columbia, 2360 East Mall, Vancouver, BC, V6T1Z3, Canada*

‡ *Department of Chemical Engineering, Delft University of Technology, Julianalaan 136, 2628 BL Delft, The Netherlands*

▪ ABSTRACT

Surface modification of cellulosic paper is demonstrated by employing plasma assisted atomic layer deposition. Al_2O_3 thin films are deposited on paper substrates, prepared with different fiber sizes, to improve their barrier properties. Thus, a hydrophobic paper is created with low gas permeability by combining the control of fiber size (and structure) with atomic layer deposition of Al_2O_3 films. Papers are prepared using Kraft softwood pulp and thermomechanical pulp. The cellulosic wood fibers are refined to obtain fibers with smaller length and diameter. Films of Al_2O_3, 10, 25, and 45 nm in thickness, are deposited on the paper surface. The work demonstrates that coating of papers prepared with long fibers efficiently reduces wettability with slight enhancement in gas permeability, while on shorter fibers, it results in significantly lower gas permeability. Wettability studies on Al_2O_3 deposited paper substrates, have shown water wicking and absorption over time only in papers prepared with highly refined fibers. It is also shown that there is a certain fiber size at which the gas permeability assumes its minimum value, and further decrease in fiber size will reverse the effect on gas permeability.

KEYWORDS: plasma-assisted atomic layer deposition, Al_2O_3 ALD, cellulose paper, hydrophobicity, water vapor transmission rate, pulp refining.

▪ INTRODUCTION

Advances in our understanding of properties of cellulosic wood fibers and increasing environmental concerns over sustainability and end-of-life disposal challenges have created a new field of research to engineer paper substrates as potential replacements for synthetic plastics. Development of the next generation of cellulosic based materials with new applications in diverse areas, ranging from food packaging to microelectronics and biomaterials, requires techniques that can modify the functionality of cellulose fibers while maintaining desired substrate characteristics. Cellulosic paper serves as a promising candidate for the development of a versatile, lightweight and environmentally friendly composites. However, it is hydrophilic and hygroscopic, which makes it difficult to beat the success of synthetic plastic materials without further modification. A wide range of studies have examined surface alteration approaches to modify and tune barrier properties of cellulosic surfaces [1-11]. These methods involve morphological and chemical modifications by plasma processing [1-3], deposition of organic and inorganic coatings [4,8], chemical vapor deposition [9], and polymerization techniques [10]. While these techniques offer superhydrophobic and superamphiphobic properties on cellulosic substrates, some may result in non-uniform coatings, surface damage of the cellulose substrate, and reduction in strength properties.

Atomic layer deposition (ALD) is a chemically versatile, layer by layer thin film deposition process which has been widely employed to deposit thin films of various materials [8, 12, 13]. The advantages of ALD rely on the self-limiting chemical reactions of the precursors on the surface of the substrate, allowing for controlling film thickness at atomic level [12]. This method is proven to create densely packed and uniform films with low defect density, precise

thickness, and low impurity contamination [12-15]. In addition, ALD is a dry method. The waste and by-products generation are very low with this technique and the coatings require no thermal drying which is an energy intensive process [12, 16]. Studies have shown that ALD coatings are perfectly suited to produce high performance permeation barriers on polymeric and porous materials, such as poly (2, 6-ethylenenaphthalate), polylactide (PLA), polyimide, polyethylene films, coated boards, and etc. [14, 17-21]. In this regard Al_2O_3 is one of the widely studied materials grown by ALD to improve oxygen and moisture barrier properties of synthetic and bio-based plastics, biopolymers, and fiber-based materials [18, 21, 22]. More specifically, the studies for Al_2O_3 films grown by ALD on paper-based products have been limited to the gas diffusion barrier performance of various (1) coated paperboards ((board basis weights between 200-310 $g \cdot m^{-2}$) coated with polylactide, galactoclugomannan, and polyethylene (coating basis weight ranging from 15-35 $g \cdot m^{-2}$)), (2) pigment coated and calendared high gloss paper (60 $g \cdot m^{-2}$) (3) polyethylene coated paper (4) commercial uncoated copy paper (80 $g \cdot m^{-2}$) and (5) nanofibrillated cellulose (60 $g \cdot m^{-2}$) [18, 21, 22]. It is shown that Al_2O_3 deposited films improved the oxygen and water vapor barrier performance [18, 21, 22]. Accordingly, the lowest water vapor transmission rate (WVTR) for paperboards and paper samples are reported for polylactide-coated boards with 25 nm Al_2O_3 deposition with value of 1±0.2 $g \cdot m^{-2} \cdot day^{-1}$ (at 23°C and 75% relative humidity (RH)) and for polyethylene (LDPF) coated papers with 50 nm Al_2O_3 deposition with value of 3.1 $g \cdot m^{-2} \cdot day^{-1}$ (at 23°C and 75% RH) respectively [18, 21]. It is also reported that 25 nm coatings of Al_2O_3 on nano-fibrillated cellulose films decreased the WVTR from ~615 $g \cdot m^{-2} \cdot day^{-1}$ to ~400 $g \cdot m^{-2} \cdot day^{-1}$ [18].

In addition to the effect of Al_2O_3 ALD coatings on gas permeability, its effect on wetting properties has been investigated [16, 18, 19, 23-25]. On the hydrophilic PLA films, PLA-coated

boards, and polyethyleneterephthalate films, the contact angles of water droplet decreased after Al_2O_3 ALD [18, 19, 25]. While results on natural cotton cellulose fibers (cotton mats and cotton balls) show that there is transition in wetting properties from hydrophilic to hydrophobic after few cycles of ALD, and as the ALD coating cycles continue the fibers return to hydrophilic state due to the formation of hydroxylated aluminum oxide [16, 24].

The effect of ALD coating on uncoated thin paper substrates free of hydrophobic binders, chemical modifiers, fillers and additives have not previously been studied. The highly porous structure of uncoated paper products has limited its use as a substrate of interest for applications where low wettability and gas permeability is required. It is known that the use of refined fibers produces paper with lower values of WVTR [26]. In this study we present an approach to the design and fabrication of hydrophobic thin paper substrates (60 $g \cdot m^{-2}$). Our hypothesis is based on that using highly refined wood fibers in conjunction with ALD will produce papers with low water vapor transmission rate comparable to that of synthetic polymeric films. Moreover, we exploit the role of fiber size through the refining energy in order to identify its optimum value for the purpose of minimizing WVTR. Therefore, we first altered the average fiber size, to control inter-fiber spacing, by mechanical refining of cellulosic fibers, and we used the refined fibers to form paper substrates. Second, we exploit plasma assisted ALD to deposit thin Al_2O_3 coating on paper substrates in order to control the inherent wetting and hygroscopic properties of the fibers. To the best of our knowledge, this is the first report of engineered hydrophobic paper substrates – free of coatings, chemicals, and additives present in commercial paper products– with WVTR values as low as 2.1 $g \cdot m^{-2} \cdot day^{-1}$ by employing plasma assisted ALD.

- **EXPERIMENTAL METHODS**

Pulp Refining. Micron-size cellulose fibers were prepared by mechanical treatment of wood pulp using refiner. Refining is a common technique used to render wood fibers suitable to improve the uniformity and strength properties of paper products [27]. During the refining process the pulp passes through the refiner plates that compress and shear the wetted fibers, thereby ripping and fibrillating the individual wood fibers [27]. In this study, Bleached Softwood Kraft Pulps and Thermo-Mechanical Pulps (TMP) were obtained from a pulp and paper mill in central British Columbia. The pulps were refined in two optimized stages at the pilot plant in Pulp and Paper Centre at the University of British Columbia (Vancouver, B.C., Canada). The detailed procedure is described elsewhere [28]. During the process, the pulp was refined between two parallel grooved plates, called rotor and stator (Fig. 1) [29].

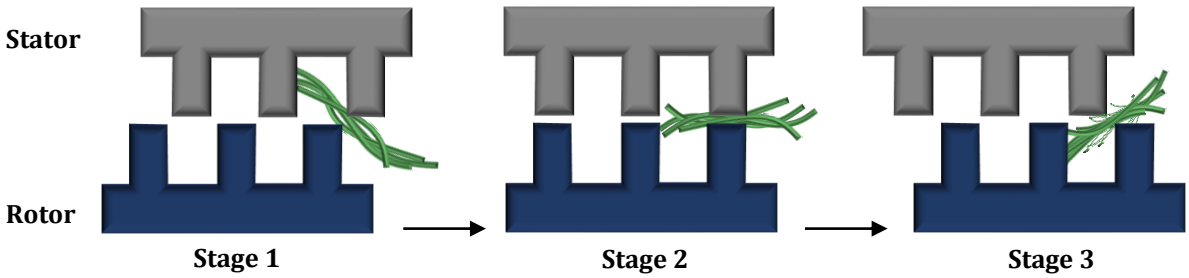

Figure 1. Primary steps of refining process

Generally, the refining process is performed in three main stages shown in Fig.1. During the first stage, which is called fiber pick up stage, the fibers in the pulp slurry of consistency of 3.4%, (pulp consistency is defined as the [oven dried weight of pulp/ (weight of pulp + water)] ×100), are collected and trapped between the edges of the plates' bars. In the second stage, the fibers are compressed by the surface of rotor and stator bars and most of the water is compressed out of the fibers. Finally, fibers are altered by shear forces resulting in the delamination of the fiber's cell wall [29]. The amount of refining is described by

evaluating the amount of energy given to the fiber by refiner and it is called specific refining energy (SRE, [kWh/t]). SRE can be calculated by dividing the net power by the fiber mass flow rate [29]. In this study, different fiber sizes were obtained subjected to varying levels of specific refining energies. The results here present three fiber sizes for softwood Kraft pulps and two fiber sizes for thermo-mechanical pulps summarized in Table 1. For the ease of reference, the handsheets prepared with these pulps are addressed as Kraft Unrefined (KU), Kraft Refined 1 (KR_1), Kraft Refined 2 (KR_2), TMP Unrefined (TU), and TMP Refined (TR).

Table 1. Refined and unrefined fiber sizes

Handsheet Type		Fiber Size (μm)
Kraft-Unrefined	KU	882
TMP-Unrefined	TU	520
TMP-Refined	TR	142
Kraft-Refined 1	KR_1	457
Kraft-Refined 2	KR_2	245

It is known that the refining process influences the structural properties and surface chemical composition of fibers [28, 29]. Specifically, the extent of refining significantly affects the cellulose fiber morphology and network in the handsheet. In this study, refining at different specific refining energies enabled us to control the fiber length and diameter, and consequently the fiber-fiber bonding and porosity of the handsheets. Fig. 2 presents the SEM images of cellulosic fibers before and after refining. Figure 2 (a) and (b) show KU and TU fibers. TMP fiber and kraft softwood fibers at the onset of delamination and fibrillation can be also seen in Fig. 2 (c) and (d) respectively. The arrows show fibrils as well as fracture and delamination of the fiber wall. Fig. 2 (e) and (f) show refined fibers of KR_1 and KR_2 respectively that have been used in this study. The increase in refining energy results in

increase of the external surface area of the fibers, which enhances the bonding ability of fibers due to the increase of hydrogen bonding [30].

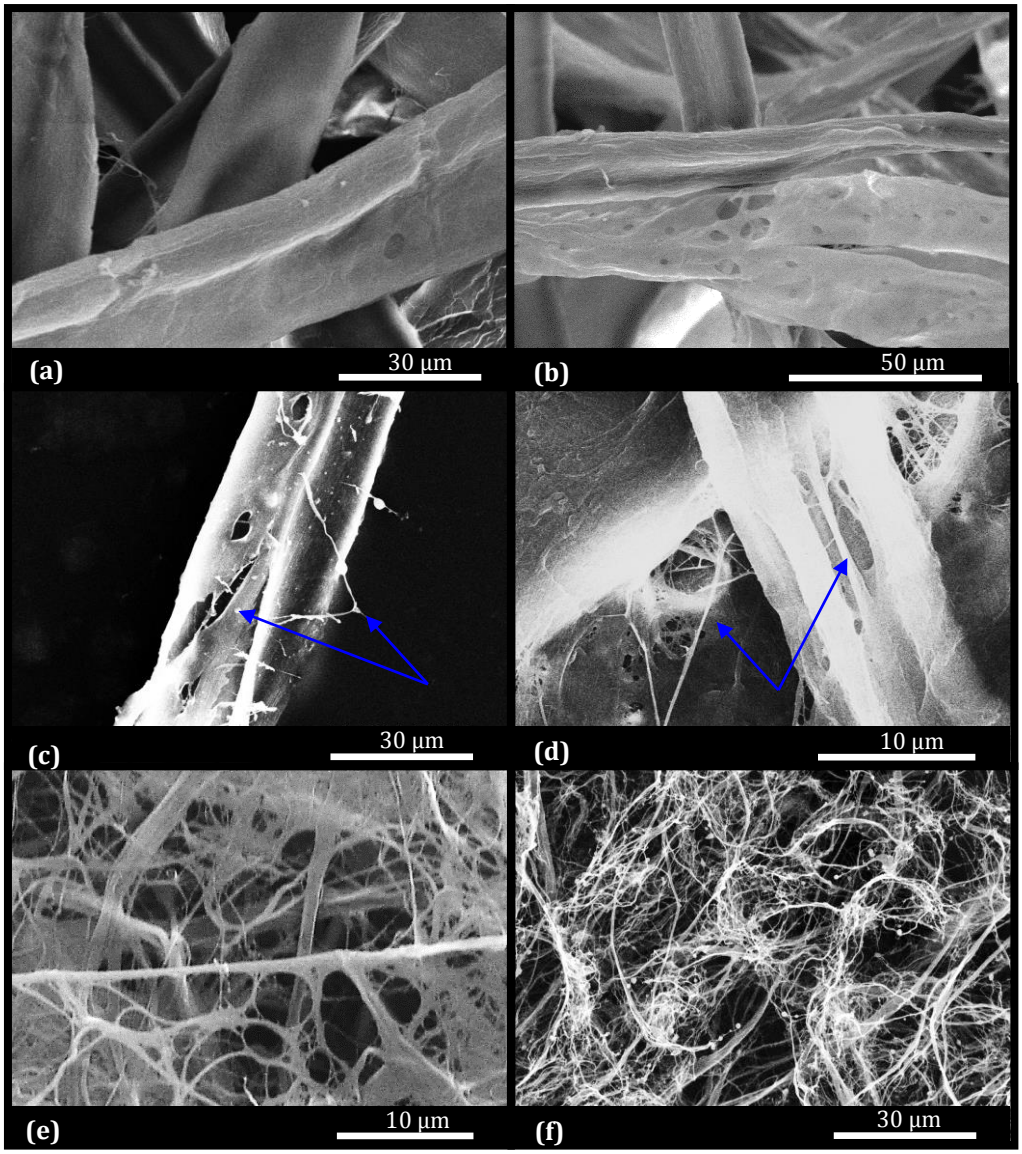

Figure 2. SEM images of (a) Kraft-Unrefined fibers (KU) (b) TMP-Unrefined fibers (TU) (c) TMP fiber at onset of fibrillation (d) Kraft fiber at onset of fibrillation (e) KR_1 fibers (f) KR_2 fibers

Cellulosic Handsheets Preparation. In order to control the effect of treatments solely on fiber/fiber network, we fabricated our own paper substrates. These substrates are free of hydrophobic binders, chemical modifiers, fillers, and additives, present in commercial papers products, which can interfere with, or mask the effect of Al_2O_3 deposition. Therefore,

the paper substrates in this study consist of only softwood natural fibers and referred to as handsheets in this manuscript. The handsheets were prepared using two different procedures. For the unrefined pulps, the sheets were prepared using a modified former on an applied vacuum [3]. The former utilizes a simple filtration of pulp suspensions through a forming fabric mesh. However, for refined pulps, a different procedure had to be used. Using the handsheet former with refined pulps will result in low retention of fibers due to the small size of the fibers which will easily pass through the forming fabric mesh. Therefore, the sheets were prepared by a casting and drying method. In this method, a pulp suspension with consistency of 1% was placed under vacuum and stirred for 15 min. The suspension was slowly transferred into a petri dish followed by manual shaking to remove any entrained air. Then the suspension was dried at ambient temperature and humidity to form cellulosic handsheets. All handsheets in both methods were prepared with basis weight of 60 $g \cdot m^{-2}$. The handsheets were kept at 23 °C and 50% RH before the treatment.

Plasma Assisted Atomic Layer Deposition of Al_2O_3. The Al_2O_3 films were grown on paper substrates by the atomic layer deposition (ALD) technique using trimethylaluminum (TMA) (97%, Sigma Aldrich) and O_2 plasma as precursors. Prior to Al_2O_3 deposition the handsheets were purged with N_2 gas in order to remove possible surface contaminants. The depositions were performed at 100°C in a FlexAL ALD reactor (Oxford Instruments, base pressure 10^{-7} mbar) equipped with a remote inductively coupled plasma (ICP) source. An ALD cycle consists of a 0.75 s pulse of TMA exposure and a 2.5 s pulse of O_2 plasma. After every precursor pulse, the reactor is purged by an N_2 flow for 3 s to remove the unused precursor and reaction by-products. Under these experimental conditions, the growth rate of Al_2O_3 was 0.14 nm/cycle. The number of ALD cycles was adjusted according to the desired Al_2O_3

coating thicknesses of 10, 25, and 45 nm. Due to the porous structure of handsheets the actual thickness of coating was estimated by measuring the thickness of the Al_2O_3 layers deposited on Si substrates under the same experimental conditions (i.e., temperature, number of cycles). This thickness measurement was performed using *ex situ* spectroscopic ellipsometry.

It should be noted that the existence of functional groups on the substrate plays an important role on the initial growth and nucleation of Al_2O_3 films by ALD [25]. Therefore, the hydroxyl groups on cellulose substrates secure a good adhesion to the deposited Al_2O_3 films with high chemical and thermal stability.

Characterization of Cellulose Handsheets. *Fiber Size Measurements.* The average fiber size distribution in the wood fiber suspension was measured with the use of the Scircco 2000 Malvern Mastersizer (Malvern Instruments Inc., Malvern, UK). The device uses static light scattering, and the particle size is reported as a volume equivalent sphere mean diameter. The device size detection limit is within 0.02 to 2000 μm. The reported fiber size in this study is the average of five measurements and the errors associated with them are within ±4 μm to ±10 μm.

Contact Angle Measurements. The advancing and receding contact angles ($\theta_{Adv.}$ and $\theta_{Rec.}$) were obtained by the "add and remove" volume method demonstrated in our previous work [3, 31]. A 3 μL water droplet with dispense rate about 0.2 μL/s was used for dynamic contact angle measurements. Static contact angles were determined by dispensing a 2 μL distilled deionized water droplets (resistivity of 18.2 MΩ·cm at 25 °C, a total organic C content of <10 ppb, and pH 7) on paper substrates with a piston-driven air displacement pipet. The image

of a water droplet on the substrate was captured with a high resolution camera (Nikon D90) and analyzed with FTA32 version 2.0 software. Contact angles on Al_2O_3 deposited handsheets were measured a few days after deposition. All handsheets were kept in a controlled environment away from light, humidity, and contaminations prior to contact angle measurements.

Water Vapor Transmission Rate. The water vapor transmission rate of the handsheets was measured by the cup method at 23 °C and 50% RH. In this method, a paper sample was cut into 1.6 cm diameter disc, then sandwiched between two rubber washers (0.9 cm aperture) and mounted on a vial filled with anhydrous calcium chloride. A screw-cap with an aperture of 1.1 cm tighten on the vial, compressing the washers against the vial to secure good sealing. The paper disc was about 1 cm above the calcium chloride desiccant. The weight of the whole set up increased as water vapor transported through the paper sample and absorbed by desiccant. All samples were preconditioned at the controlled environment for 48 hours prior to measurements. The weights were tracked for 10 days and the average values are reported. The Water Vapor Transmission Rate (WVTR) and Water Vapor Permeability (WVP) were calculated according to equations 1 and 2:

$$WVTR\ (\mathrm{g \cdot m^{-2} \cdot day^{-1}}) = \frac{\Delta m\ (\mathrm{g})}{A\ (\mathrm{m^2})} \tag{1}$$

where Δm is the difference between the initial mass (g) and the mass after 24h (g), and A is the exposed area of paper sample.

$$WVP\ (\mathrm{g \cdot Pa^{-1} \cdot m^{-2} \cdot day^{-1}}) = \frac{WVTR\ (\mathrm{g \cdot m^{-2} \cdot day^{-1}})}{P_s\ (\mathrm{Pa})(RH_1 - RH_2)} \tag{2}$$

where P_s is the saturation vapor pressure (28.1 kPa at 23°C), RH_1 is the relative humidity of condition room expressed as a fraction (0.5) and, RH_2 is the relative humidity in the vial expressed as a fraction (0).

Air permeability. The air resistance of handsheets was evaluated by the Gurley method. This method measures the time (s) that is required for 100 mL of air to pass through the handsheets at pressure of 1.22 kPa. The TAPPI standard method of T460 om-02 was followed for the measurements. The tests were performed at 23°C and 50% RH.

Profilometer Measurements. Roughness measurements were conducted using the Wyko NT1100 Optical Profilometer. The average roughness values (R_a) were analyzed using the Vision software (Veeco Instruments Inc.). The reported values in this study are the average values for three measurements.

SEM Imaging. The surface structure and morphology of cellulosic fibers and films before and after ALD deposition were examined with a Hitachi S-3000N-VP scanning electron microscope at operating voltage of 5-10 kV. All images were obtained at variable pressure mode since paper and Al_2O_3 films are insulators.

XPS Analysis. The elemental composition of the material surface was determined by X-ray photoelectron spectroscopy. The spectra were collected by the Leybold model MAX200 XPS with Al K-α X-rays and 15 kV, 20 mA emission current. The analyzed area for all samples was 4×7 mm^2 with the X-ray spot size of ~ 20 mm diameter. The pass energies to measure the survey scan and narrow scan were 192 eV and 48 eV respectively.

FTIR-ATR Analysis. Fourier transform infrared spectra (FTIR) with attenuated total reflectance (ATR) were obtained with the Thermo Niccolet AVATAAR 360 FTIR

spectrometer. The 0.5×0.5 cm cut samples were pressed against the ATR crystal using a flat metal with controlled pressure. The level of pressure kept constant for all test spices.

- **RESULTS AND DISCUSSION**

Effect of Al_2O_3 ALD on Wettability. Film Thickness Effect. It is well established that low surface energy and surface roughness are the main parameters responsible for hydrophobic and superhydrophobic surfaces [1-3]. The equilibrium contact angle formed by a liquid on an ideal, perfectly smooth, and chemically homogenous surface is represented by the Young's equation (Eq. 3):

$$\cos\theta_Y = \frac{\gamma_{SV}-\gamma_{SL}}{\gamma_{LV}} \quad (3)$$

where γ_{SV}, γ_{SL}, and γ_{LV} are solid/vapor, solid/liquid, and liquid/vapor surface free energy per unit area [32]. According to Young's equation, the contact angle is higher on surfaces with lower surface free energy (i.e., lower γ_{SV}). Paper is composed of a random network of fibers. Therefore, its wettability is not only dictated by the surface free energy, but also by the morphology of the surface which plays an important role. In order to account for the morphology of the surface, the two commonly cited models used for wetting on rough surfaces are the Wenzel [33] and the Cassie-Baxter [34]. The Wenzel model is for a homogeneous wetting regime where the fluid follows the morphology of the surface, filling the roughness grooves of the surface (creating a non-composite interface). Therefore, the roughness of the surface enhances both hydrophobicity and hydrophilicity. In the Cassie-Baxter model, the fluid exhibits a composite or heterogeneous wetting regime. In this state the droplet is supported by air pockets trapped between asperities of the surface which reduces the liquid-solid contact area.

Prior to Al_2O_3 deposition all handsheets were hydrophilic. More specifically, the static water contact angles on KU and TU handsheets can be considered practically to be zero, since the droplet quickly absorbs and wicks onto the sheet upon contact. For KR and TR handsheets, due to their denser structure, it takes time for a droplet to totally absorb. The static water contact angles on KR and TR are between 10°-20°, immediately after the droplet dispensed on the surface. The deposition of Al_2O_3 films on handsheets renders them hydrophobic. To fully characterize and understand the effect of film thickness on the barrier properties of handsheets, we have studied three coating thicknesses of 10, 25, and 45 nm. The results for the advancing contact angles and the contact angle hysteresis (CA_H) (the difference between the advancing and receding contact angle values) of the three different film thicknesses are presented in Fig. 3. In this study, the aim was to deposit Al_2O_3 on one side of the sheets; however, the film growth on the other side could not be prevented and resulted in hydrophobic surfaces on both sides of the sheets. According to the results, the hydrophobicity of the handsheets was shown to slightly increase with Al_2O_3 film thickness. This is more significant for unrefined Kraft and TMP handsheets in comparison with handsheets formed with refined pulp fibers. As Fig. 3 demonstrates, handsheets with refined pulp fibers are relatively unaffected by the increase of the coating thickness.

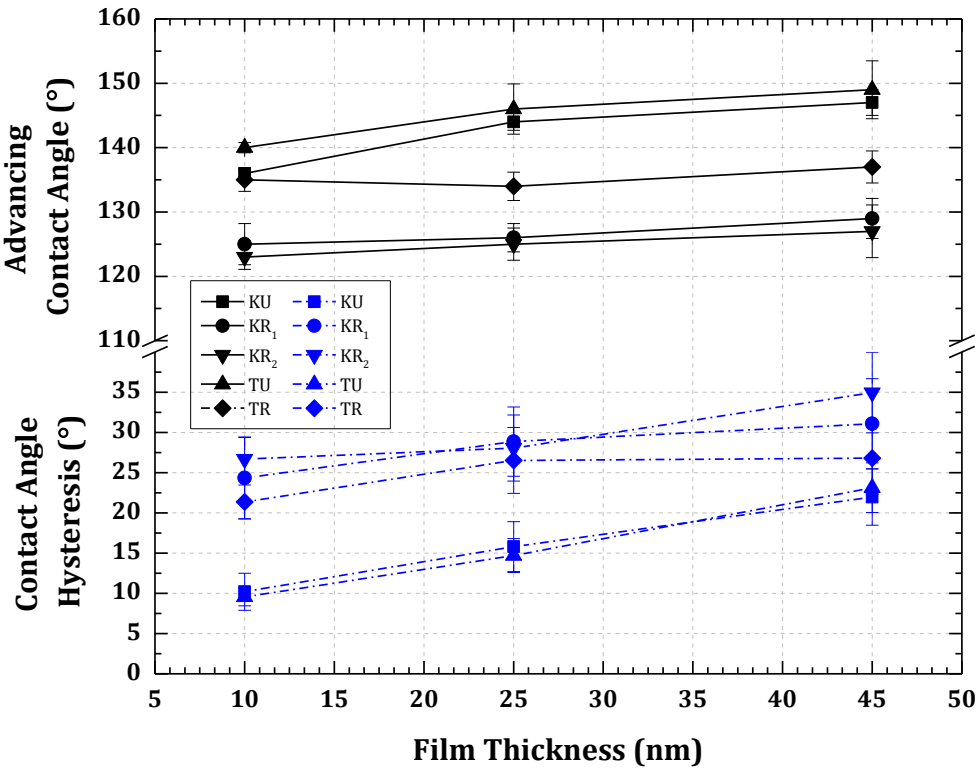

Figure 3. Advancing contact angles and contact angle hysteresis for handsheets after Al_2O_3 ALD at different film thicknesses.

The effect of Al_2O_3 ALD (at deposition temperatures of 60° and 90°) on the wettability of woven cotton mats and cotton balls was reported by Lee et al. [16], showing that there is a wetting transition from hydrophilic to hydrophobic after the first few ALD cycles (2-3 cycles). However, the surface transitioned back to the hydrophilic state after about 15 ALD cycles. In our study we observed a distinctly different behavior for the cellulosic wood fiber handsheets. There was no transition from hydrophobic to hydrophilic state with increase of ALD cycles. We observed an increase in contact angle for KU and TU handsheets from 10 nm to 25 nm thicknesses which corresponds to 75 and 190 ALD cycles, respectively. However, for a coating thickness of 45 nm (300 cycles) the increase in contact angles is insignificant compared to that of 25 nm coating thickness. For handsheets with refined pulps (KR and TR), on the other hand, the increase in contact angle is small (about 1-2 degrees which is within

experimental error) with increase of ALD cycles. On the contrary to advancing contact angles, the effect of film thickness is more evident on contact angle hysteresis as its value increases significantly with film thickness (specially on unrefined samples). This is due to the decrease of handsheet surface roughness (which is discussed further in the next section) as the film thickness increases. It is established that the contact angle hysteresis depends on chemical heterogeneity and surface roughness [35]. Therefore, although the increase of film thickness slightly enhanced the hydrophobicity of the handsheets, its effect on surface roughness by reducing it has resulted in higher contact angle hysteresis values.

Fig. 3 also illustrates that the contact angles on handsheets prepared with unrefined pulps (KU, TU) are higher than those of the refined pulps (TR, KR_1, and KR_2). Highly refined samples (KR_1 and KR_2) resulted in lowest contact angles after Al_2O_3 deposition. This behavior is attributed to the fact that refining results in higher specific surface area which in turn increases the number of fiber-fiber bonds. Therefore, during sheet formation the strong hydrogen bonding between the fibrils causes formation of a dense, nonporous, and smooth surface for highly refined samples. The relative reduced roughness causes the decrease of contact angle which is expected based on Wenzel equation. Fig. 4 illustrates advancing contact angles vs. fiber size.

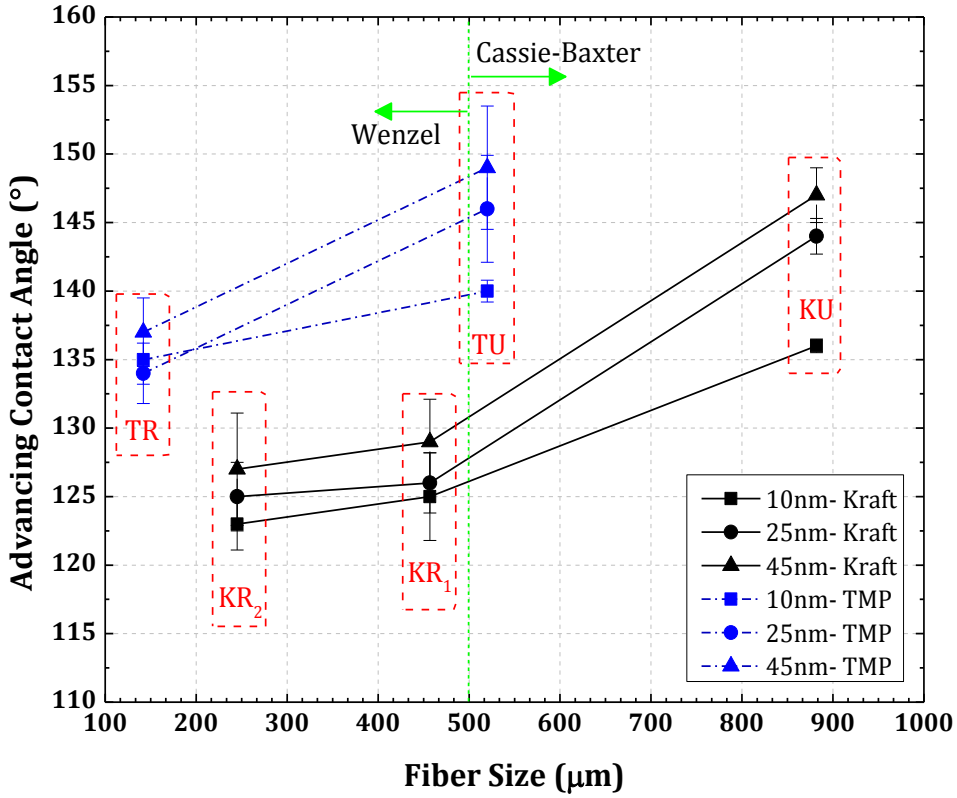

Figure 4. Effect of fiber size on wetting transition for handsheets with TMP and Kraft Pulp for the three film thicknesses.

Depending on the fiber size, the handsheets are either in the Wenzel or in the Cassie-Baxter wetting state. In order to test our hypothesis, a 2 μL stained water droplet was dispensed on the surface of the handsheets, and it was removed off the surface after 20 s by letting the droplet wicks into a Kimwipes. The stained water droplet on KU and TU could be removed without leaving any residual fluid on the handsheets that is visible by unaided eye. However, on TR, KR_1, and KR_2 (handsheets made with refined pulps) surfaces, water droplets pinned on the surface even after inversion, and the stain of water droplet remains on the surface when the droplet is removed. This implies that the droplet resides on the handsheet according to the Cassie-Baxter state for KU and TU handsheets. On the other hand, on TR, KR_1, and KR_2 the droplets reside in the Wenzel wetting state, leading to higher adhesion to the fibers. Fig. 5 shows the stain of water droplet on the surface of handsheets

using inverted fluorescent microscope. We stained the water with rhodamine (which is fluorescent) and took the images of the handsheets surface after withdrawing the droplet. The homogeneous wetting on KR_2 handsheet is evident based on Fig. 5 (a). As mentioned, macroscopically we did not observe stain residues on KU handsheet, but microscopically there is an evidence of droplet pining on the very surface layer of the fibers. The smaller contact area that is formed by stain of the droplet on KU handsheet (for 25 nm Al_2O_3 thickness) and the heterogeneous coverage of stain on the surface confirms the Cassie-Baxter wetting state on these handsheets.

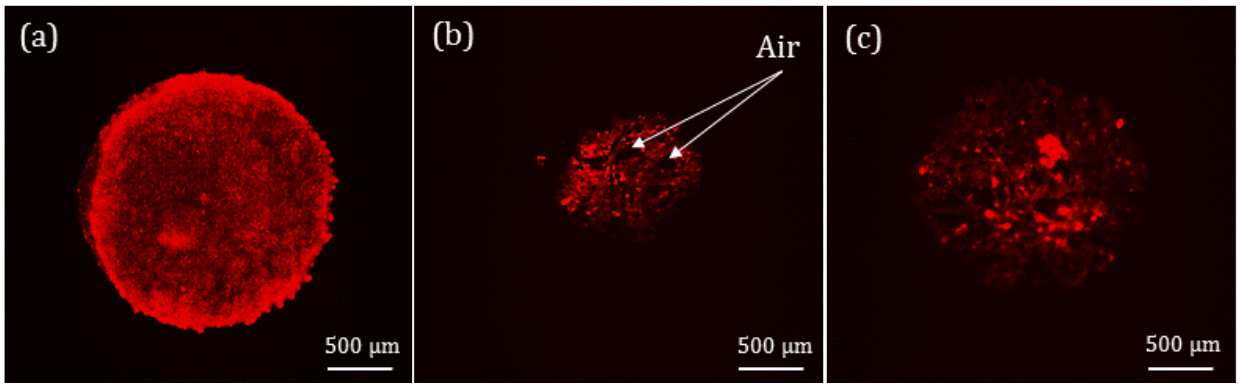

Figure 5. Stain of water droplet on (a) KR_2 handsheet with 25 nm Al_2O_3 (b) KU handsheet with 25 nm Al_2O_3 and (c) KU handsheet with 10 nm Al_2O_3.

The long term stability of contact angles also prove the wetting state hypothesis. Fig. 6 illustrates the static contact angles on handsheets with Al_2O_3 film thickness of 10 nm. The images of a water droplet were captured every minute up to 20 min. In order to minimize the evaporation effect, the droplet was covered, and the cover was removed only at the time of capturing the image. According to the results, on KU and TU handsheets the droplet shape remains stable over time and the slight decrease in contact angle, due to evaporation, is within the range of hysteresis contact angle results shown in Fig. 3. On handsheets with refined pulps, the contact angles decreased over time. According to Fig. 6 the decrease of

contact angle for KR_1 and KR_2 samples is about 40° over 20 min which is significantly higher than their hysteresis contact angle values reported in Fig 3. Specifically, after about 13 min, the handsheets are not hydrophobic anymore and have contact angle of about 87°. Since the droplets are in the Wenzel wetting state, there is higher adhesion of water droplet to the fibers. Therefore, over time the liquid may come into contact with underlying fibers and absorb into the substrate, causing the decrease of contact angles. Therefore, for refined samples the decrease of static contact angles can be mainly due to wicking and absorption over time.

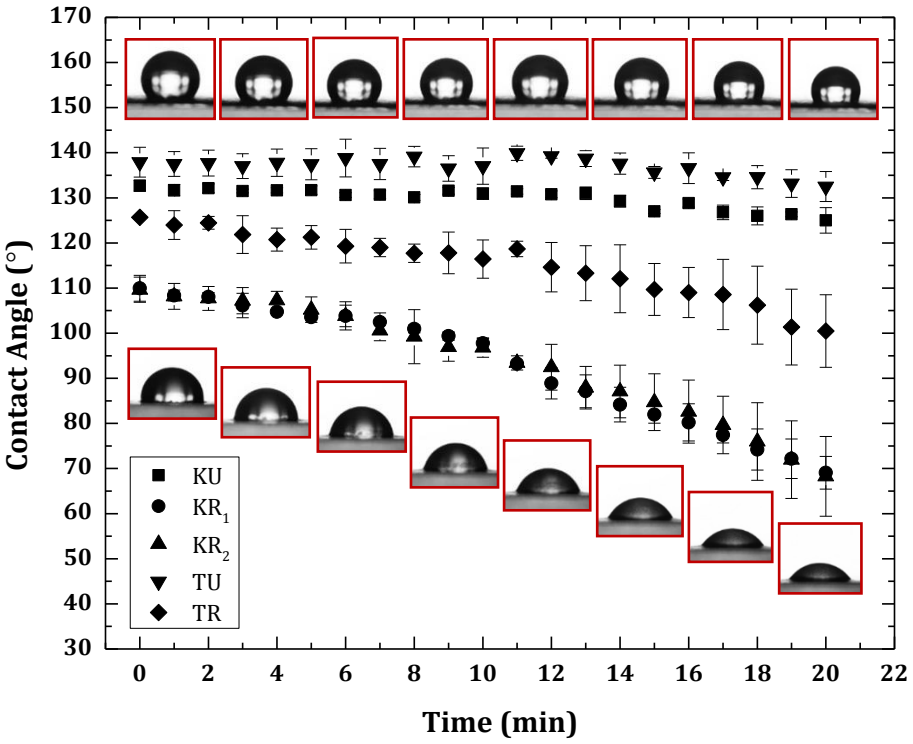

Figure 6. Long term static contact angles on handsheets with an Al_2O_3 film thickness of 10 nm.

The Al_2O_3 ALD coated handsheets are not noticeably different from the original unmodified handsheets, having similar feel and flexibility. The SEM and profilometer images of handsheets coated with 25 nm Al_2O_3 are shown in Fig. 7. The shorter fiber size results in

a decrease of the handsheet porosity and individual fibers become harder to identify. For the refined pulp handsheets, the increase of surface area and higher number of hydrogen bonds between the fibrils creates aggregates that fill the pores in the fiber network leading to a smoother appearance of the handsheets [2].

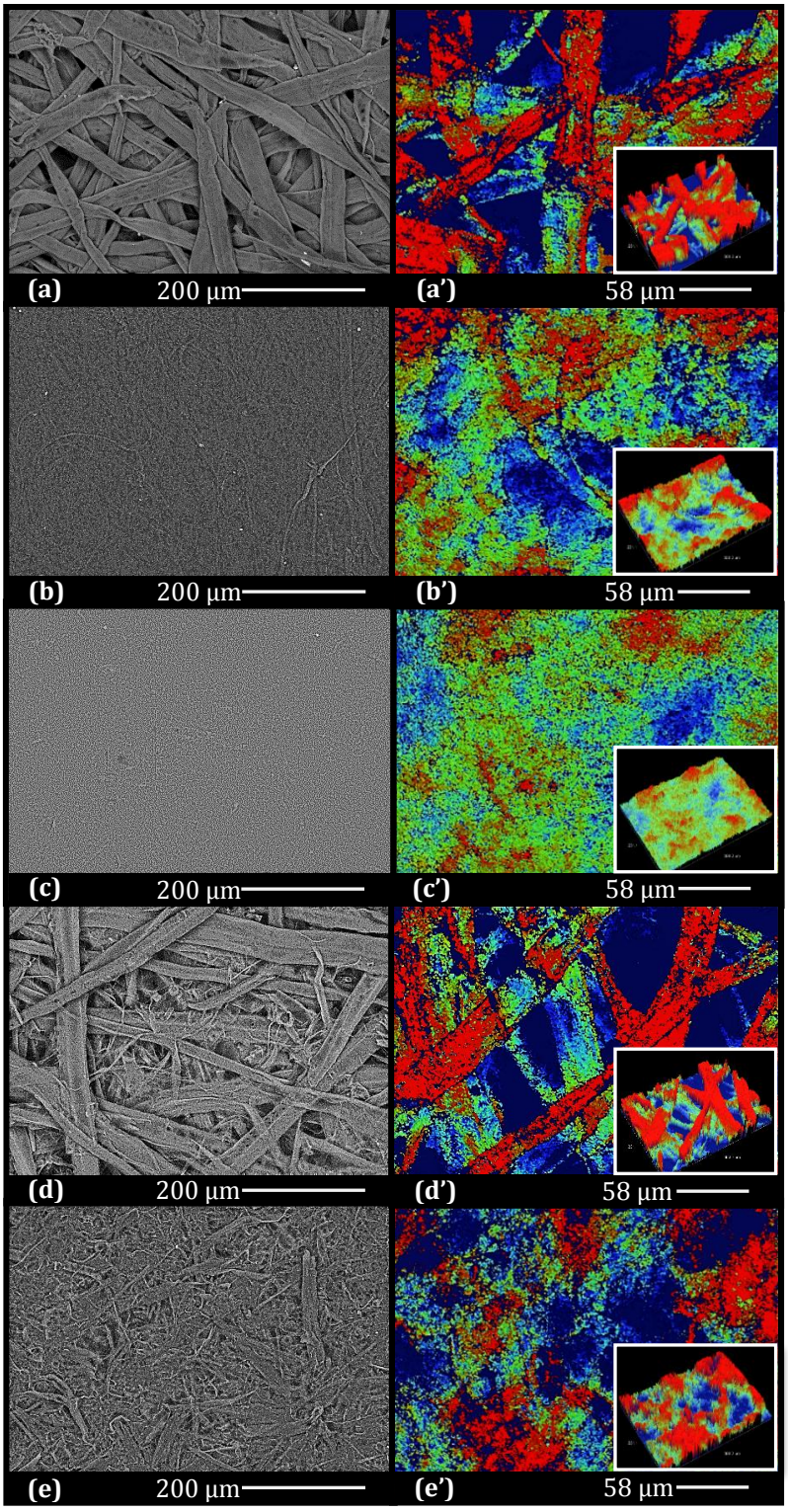

Figure 7. Profilometer images (right) and complementary SEM images (left) of handsheets prepared from (a, a') KU (b, b') KR_1 (c, c') KR_2 (d, d') TU (e, e') TR.

According to Fig. 3 and 4, the handsheets prepared by TMP pulps show higher contact angles than the Kraft pulps. This is due to the presence of hydrophobic substances such as lignin and extractives on TMP fiber surface. The wood fibers may consist of different amounts of cellulose, lignin, hemicellulose, and extractives depending on the pulping technique and this influences their wettability [3, 36, 37].

Roughness Effect. As mentioned earlier, Al_2O_3 films on handsheets create a low energy surface, which renders the handsheets hydrophobic. However, the roughness of the handsheets highly affects the contact angle values. Table 2 presents the average surface roughness (R_a) before and after the Al_2O_3 deposition for refined and unrefined handsheets. According to Table 2 the roughness of the sheets is highly dependent on fiber size and coating thickness.

Table 2. Profilometer roughness values of handsheets before and after Al_2O_3 deposition

Handsheet Type	Fiber Size (μm)	Average Roughness Values (R_a) (μm)			
		Uncoated	10 nm	25 nm	45 nm
KU	882	9.3 ± 0.2	8.2 ±0.6	7.1 ± 0.5	6.3 ±0.1
TU	520	8.7 ± 0.5	7.9 ± 0.8	7.0 ±0.4	6.2 ± 0.7
TR	142	3.5 ± 0.3	3.4 ± 0.3	3.2 ± 0.1	2.9 ± 0.4
KR_1	457	2.5 ± 0.1	2.5 ± 0.1	2.2 ± 0.3	2.1 ± 0.3
KR_2	245	1.7 ± 0.1	1.7 ± 0.1	1.2 ± 0.1	1.3 ± 0.1

Fig. 8 shows that handsheets with unrefined pulp (KU) resulted in the highest advancing contact angles due to the higher roughness, which is expected based on the Wenzel and the Cassie-Baxter wetting models. This is consistent in all three film thicknesses. However, as the coating thickness increases, it leads to lower roughness values and smoother surfaces which results in an increase in the contact angle hysteresis. Higher film thickness also results in higher coverage of surface by Al_2O_3 film and loss of porosity.

The higher contact angles of KU handsheets could be also due to the effect of free hydroxyl groups on the KU handsheets before deposition of Al_2O_3.

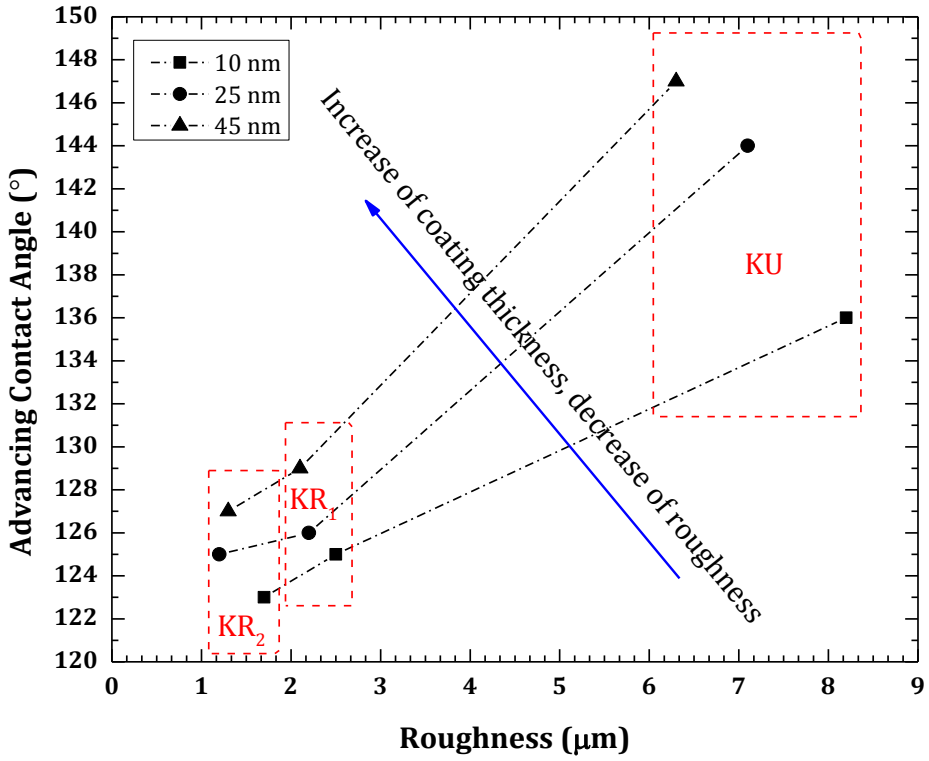

Figure 8. Effect of handsheet's roughness on advancing contact angles ($\theta_{Adv.}$) for handsheets prepared by Kraft pulp.

More specifically, the FTIR-ATR results (Fig. 9) on untreated samples reveal a higher number of hydroxyl (-OH) groups on unrefined pulp (KU) handsheets at peak wavenumber of 3327 (cm^{-1}). The band intensity of –OH peaks decreased for KR_1 and decreased further more for KR_2 handsheets. This is due to the fact that refining increases the number of hydroxyl groups on the fiber surface, and consequently increases the hydrogen bonding between the fibers during handsheet formation [30] (i.e. higher number of –OH groups at the surface of the fiber get involved in interfibrillar hydrogen bonding, which causes formation of low porosity sheets). Therefore, according to the FTIR-ATR results, unrefined fibers have large number of free or unbonded hydroxyl groups on the surface, which are more accessible

for reaction with Al_2O_3. It is known that the higher the number of free hydroxyl groups on a surface, the more the surface is prone to modification. Based on this, we believe the higher contact angles of KU handsheets is due to the presence of more free/unbonded –OH groups available to react with Al_2O_3 compared to the case of refined samples with lower number of free –OH groups.

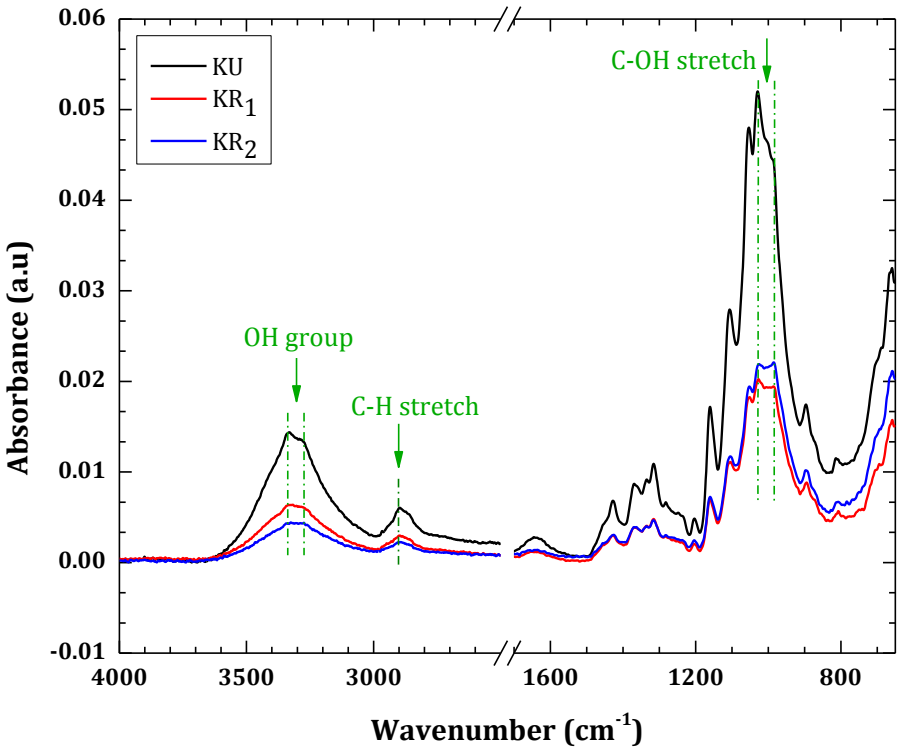

Figure 9. FTIR-ATR spectra on bare (untreated) Kraft pulp handsheets

The surface chemistry of plasma assisted Al_2O_3 ALD using infrared spectroscopy on pure Al_2O_3 films shows dependency of the surface groups to the deposition temperature [38]. Basically, the study [38] shows at lower deposition temperature (25°C), the number of hydroxyl groups on the surface created by O_2 plasma increased compared to depositions at 100° and 150°C.

In this study, XPS was employed to identify the elements and chemical bonds on the surface of uncoated and Al_2O_3 coated handsheets. The survey scan spectra of an untreated handsheet mainly show the presence of oxygen (O_{1s}: 27.09%) and carbon (C_{1s}: 70.83%) elements with oxygen to carbon (O/C) ratio of 0.38. The existence of chemical bonds on the surface was determined by high resolution XPS carbon (C_{1s}) spectra. The resulting deconvoluted three major peaks of C_{1s} for untreated and 10 nm Al_2O_3 deposited handsheets are shown in Fig. 10 (a) and (b) respectively. The C_1 peak at 285.0 eV corresponds to carbon-carbon (C-C) or carbon-hydrogen (C-H) bonds, the C_2 peak at 286.6 eV is due to bonding of carbon to a single non-carbonyl oxygen (C-O), and the C_3 peak at 288.0 eV represents bonding of a carbon atom to one carbonyl oxygen (C=O) or to two non-carbonyl oxygens (O-C-O). The three peaks are consistent with the literature data for cellulose [3, 23, 39]. The intensity of C_1, C_2, and C_3 peaks decreases after 10 nm Al_2O_3 ALD deposition (Fig. 10 (a) and (b)). It should be noted that the C_3 peak on an uncoated handsheet shifts to a higher binding energy of 289 eV after ALD coating which can correspond to one carbonyl oxygen and one non-carbonyl oxygen (O-C=O) bonds to carbon atom. Also, the O/C elemental ratio increased from 1.61 (10 nm coating thickness) to 1.97 for the 45 nm coating. This is due to the formation of Al_2O_3 (Al-O) which is confirmed by the O_{1s} peaks at 531.5 eV (Fig. 10 (c)). The O_{1s} peak also confirms O-C bond at 533 eV on the uncoated handsheet. After the Al_2O_3 deposition, the O-C peak position shifts to a lower binding energy consistent with oxygen binding mainly to aluminum (Fig. 10 (c)). Also, the Al_2O_3 peaks become dominant after 10 nm and 45 nm deposition. This is consistent with Al_2O_3 bonds on Al_{2p} peaks for both coating thicknesses as demonstrated in Fig. 10 (d). The intensity of the Al_{2p} peak increased with respect to increase in coating thickness. According to Lee et. al [16] the presence of Al-O-C peak at binding energy of 532.4 eV was the

reason for hydrophobicity of cellulosic cotton mats after a few cycles of ALD. Their study shows, that the formation of Al-(O-C-)$_3$ bonding units during interaction of trimethylaluminum with –OH units on cellulose surface is the reason for hydrophobicity. In addition, the air exposure of the sample after Al_2O_3 deposition caused adventitious carbon adsorption which resulted in hydrophobicity of the cotton mats even after subsequent ALD cycles [16]. Our XPS results here also shows the presence of carbon on the surface of handsheets after Al_2O_3 deposition, which could originate from the adsorption of carbon from environment or the presence of Al-O-C, which both affect the wettability of the surface.

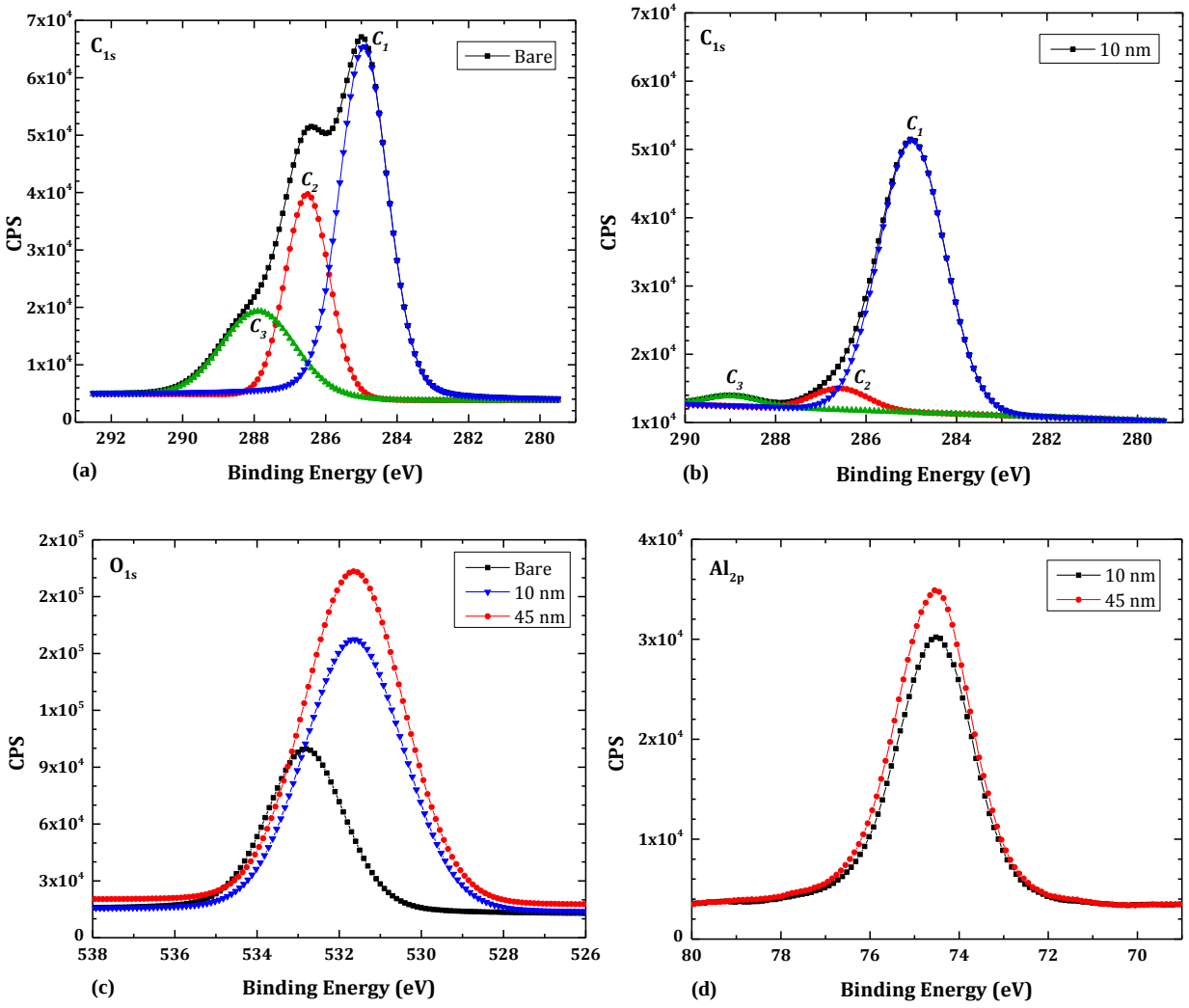

Figure 10. KR_2 handsheets' XPS high resolution spectra of (a) C_{1s} for bare sample (b) C_{1s} for 10 nm Al_2O_3 ALD (c) O_{1s} and (d) Al_{2p}.

Effect of Al_2O_3 Film Thickness on Gas Permeability

The water vapor transmission rates (WVTR) and water vapor permeability (WVP) at 23°C and 50% RH for handsheets before and after ALD modifications are presented in Tables 3 and 4 respectively. Although ALD modification greatly improves the wettability of unrefined Kraft and TMP handsheets, it did not affect their WVTR significantly. The reduction in WVTR value at 45 nm coating thickness is about 15% for KU handsheets and about 36.6% for TU handsheets. However, for refined Kraft pulp handsheets, the WVTR decreases 97% for KR_1 and 98% for KR_2 after Al_2O_3 deposition. Table 3 clearly shows the effect of fiber size on WVTR values. For both handsheets prepared by Kraft and TMP pulps the decrease in fiber size results in decrease of WVTR values. This is due to the larger surface area of fibers after refining. Accordingly, as mentioned before, the enhanced bonding between the fibers results in a dense fiber network with smaller pores and uniform dimensions [40]. Therefore, the tortuosity increases within the sheets due to the formation of this dense network, which lowers the permeability. In addition to fiber size, fiber entanglement plays an important role in the increase of tortuosity [40]. Studies have shown that nano-fibrillated cellulose (NFC) has longer fiber sizes compared to crystalline nano-cellulose (CNC) [40]. However, the gas permeability of the CNC film is higher than that of the NFC film due to the higher entanglement of fibrils within the NFC films which results in increase of the tortuosity factor [40]. The reported WVTR value (at 23°C and 50% RH) for NFC film (with thickness of 42 μm) is about 234 $g \cdot m^{-2} \cdot day^{-1}$ [7] which is higher than the WVTR values for the KR_1 and KR_2 handsheets in this work. Although KR_1 fibers are longer

than KR_2 (Table 3), the lowest WVTR value for untreated samples are for handsheets prepared with KR_1 fibers. Therefore, it can be concluded that there is an optimum fiber size that results into the lowest permeability. This can be due to the highest possible fiber entanglements that increase tortuosity and consequently reduce gas permeability to a minimum possible value.

Table 3. Water Vapor Transmission Rates for handsheets before and after Al_2O_3 ALD modification

Handsheet Type	Fiber Size (μm)	Sheet Thickness (mm)	WVTR ($g \cdot m^{-2} \cdot day^{-1}$)			
			Uncoated	10 nm	25 nm	45 nm
KU	882	0.21	694.8 ± 11.5	615.9 ± 2	606.6 ± 8.9	589.9 ± 15.1
TU	520	0.34	858.6 ± 16.1	602.1 ± 12.6	566.0 ± 10.6	544.6 ± 14.2
TR	142	0.11	640.9 ± 13.2	452.0 ± 13.5	443.2 ± 8.7	392.0 ± 11.1
KR_1	457	0.07	88.6 ± 4.6	2.3 ± 0.2	2.5 ± 0.4	2.5 ± 0.2
KR_2	245	0.06	107.1 ± 2.5	2.2 ± 0.9	2.1 ± 0.2	2.2 ± 0.5

Table 4. Water Vapor Permeability for handsheets before and after Al_2O_3 ALD modification

Handsheet Type	Fiber Size (μm)	Sheet Thickness (mm)	WVP ($g \cdot m^{-2} \cdot day^{-1} \cdot kPa^{-1}$)			
			Uncoated	10 nm	25 nm	45 nm
KU	882	0.21	49.5 ± 0.82	43.8 ± 0.14	43.2 ± 0.63	42.0 ± 1.07
TU	520	0.34	61.1 ± 1.15	42.9 ± 0.90	40.3 ± 0.75	38.8 ± 1.01
TR	142	0.11	45.6 ± 0.94	32.2 ± 0.96	31.5 ± 0.62	27.9 ± 0.79
KR_1	457	0.07	6.3 ± 0.33	0.2 ± 0.01	0.2 ± 0.03	0.2 ± 0.01
KR_2	245	0.06	7.6 ± 0.18	0.2 ± 0.06	0.2 ± 0.01	0.2 ± 0.04

The WVTR values for KR handsheets remarkably reduced after Al_2O_3 ALD compared to KU handsheets. However, there is not a significant difference in the WVTR values between the KR_1 and KR_2 handsheets after Al_2O_3 deposition. The results also show that the increase in coating thickness does not affect water vapor permeability by a great amount for KR_1 and KR_2 handsheets. Therefore, the combination of Al_2O_3 coating thickness of 10 nm and fiber sizes as small as 457 μm (as in KR_1) would be enough to achieve WVP values as low as about 0.2 $g \cdot m^{-2} \cdot day^{-1} \cdot kPa^{-1}$. It should be noted that although the refined TMP fibers have smaller

fiber size compared to refined Kraft, the WVTR values for TR sheets are significantly higher than RK sheets. This is due to the presence of lignin in TR fibers, which hinders hydrogen bonding and forms more pores, resulting in higher WVTR values [40]. As mentioned earlier, for the purpose of this study all WVTRs were obtained at 23 °C and 50% RH and the effect of treatment on handsheets at higher relative humidity were not investigated. Generally, for uncoated paper based materials at higher relative humidity, the WVTR is expected to increases due to the swelling of fibers [40].

The Gurley air permeability test was used to obtain the time required for air to pass through a unit area at a given pressure. The air permeability values for untreated and 25 nm Al_2O_3 ALD handsheets at 23 °C and 50% RH are presented in Table 5. Handsheets prepared with refined pulp fibers have remarkably lower air permeability compared to handsheets prepared with unrefined pulp fibers.

Table 5. Gurley air permeability for untreated and 25 nm Al_2O_3 ALD coatings

Handsheet Type	Fiber Size (μm)	Air Permeability (s/100cc)	
		Uncoated	25 nm
KU	882	1.3 ± 0.1	5.7 ± 0.54
TU	520	3.2 ± 0.1	17.6 ± 0.3
TR	142	222.9 ± 25.5	362 ± 20.1
KR_1	457	352800	Impermeable
KR_2	245	Impermeable	Impermeable

The trend in air permeability agrees with the WVTR results. According to table 5, the air permeability before and after treatment for the unrefined pulp handsheets (KU and TU) is in the order of few seconds. However, for KR_1 handsheets before the treatment, it takes 98 hours for the 100 cc of air to pass through the sheet. The KR_1 and KR_2 samples after 25 nm coating can be considered impermeable and the air permeability could not be quantified with

Gurley method. As mentioned earlier this is due to the decrease in fiber size as well as filling of the pores after Al_2O_3 ALD coatings which results in lower permeability.

Thus, the major finding in this work is that it demonstrates the requirements to achieve an effective water vapor barrier by: (i) use of refined fibers (reduction in fiber size) to obtain a densely packed cellulosic film; and (ii) deposition of Al_2O_3 to reduce the surface energy as well as porosity of the sheets. A major target of highest gas barrier property with the lowest number of coating thicknesses was achieved with the Al_2O_3 ALD method. A maximum water vapor barrier improvement of ~98% (WVTR value of 2.1 g· m^{-2}·day^{-1}) was determined after ALD treatment for Kraft refined handsheets. The reduction in Kraft pulp fiber sizes reduces the WVTR by 87% for KR_1 and 84% for KR_2 prior to ALD treatment. For comparative reasons the WVTR of commercially available coatings and packaging materials such as polyvinylidene chloride coated cellulose films, cellulose acetate films, and PET films are 6, 14, and 4 g·m^{-2}·day^{-1} respectively at 35 °C and 25% RH [41] which are inferior to some of the coated papers elaborated in this study. Contrary to polymers, these handsheets, regardless of the process, are produced from a renewable material. The potentials are in packaging applications and some may not be foreseen. For example, we have previously shown that by using the highly refined fibers (bare KR_1 and KR_2 samples here) we can make very thin and high electrochemically conductive separators that can be used in the design of fast charging supercapacitors [42].

CONCLUSIONS

The present study demonstrates that the use of refined wood fibers of suitable size in conjunction with atomic layer deposition of Al_2O_3 enables the fabrication of paper with a water vapor transmission rate that is superior to some of the commercially available coated

films. The permeability is greatly reduced due to the formation of dense networks within the sheets by smaller and more uniform fibers dimensions. The deposited Al_2O_3 has its maximum effect on gas permeability with the paper produced with Kraft refined pulp. We observed the lowest WVTR for cellulosic sheets prepared by 450 μm fiber sizes from refined Kraft pulp. This is due to the higher fiber entanglements within the cellulosic sheets that increase the diffusion path for gas molecules. Further refining of the cellulose fibers to 245 μm reverses the effect and caused increase in WVTR values. The coatings also effectively modified the surface energy of handsheets and converted the highly hydrophilic cellulose surface to a hydrophobic one. However, the hydrophobicity of the sheets is highly dependent on surface roughness. The fabricated sheets in this study are comparable with commercial synthetic polymers. Therefore, the preparation of hydrophobic and water vapor barriers by Al_2O_3 ALD approach on engineered paper is a promising tool in renewable material science and technology.

AUTHOR INFORMATION

Corresponding Author

*E-mail: peter.englezos@ubc.ca.

Notes

The authors declare no competing financial interest.

FUNDING SOURCES

This work is supported by the Natural Sciences and Engineering Research Council of Canada (NSERC) and Innovative Green Wood Fiber Products Strategic Network.

ACKNOWLEDGMENT

The authors thank Dr. Mark Martinez and Abbas Nikbakht at University of British Columbia for generously donating the refined pulp samples. Thanks to Masoud Daneshi for helping with fluorescent microscope images.

- **REFERENCES**

[1] Balu, B.; Breedveld, V.; Hess, D. W. Fabrication of "Roll-off" and "Sticky" Superhydrophobic Cellulose Surfaces via Plasma Processing. *Langmuir* **2008**, *24*, 4785−4790.

[2] Li, L.; Breedveld, V.; Hess, D. W. Design and Fabrication of Superamphiphobic Paper Surfaces. *ACS Appl. Mater. Interfaces* **2013**, *5*, 5381-5386.

[3] Mirvakili, M.; Hatzikiriakos, S. G.; Englezos, P. Superhydrophobic Lignocellulosic Wood Fiber/Mineral Networks. *ACS Appl. Mater. Interfaces* **2013,** *5*, 9057-9066.

[4] Stanssens, D.; Abbeele, H. V.; Vonck, L.; Schoukens, G.; Deconinck, M.; Samyn, P. Creating Water-Repellent and Super-Hydrophobic Cellulose Substrates by Deposition of Organic Nanoparticles. *Mater. Lett.* **2011**, *65*, 1781-1784.

[5] Teisala, H.; Tuominen, M.; Kuusipalo, J. Superhydrophobic Coatings on Cellulose-Based Materials: Fabrication, Properties, and Applications. *Adv. Mater. Interfaces* **2014**, *1*, 1300026.

[6] Hubbe, M. A.; Rojas, O. J., Lucia, L. A. Green Modification of Surface Characteristics of Cellulosic Materials at the Molecular or Nano Scale: A Review. *BioResources* **2015**, *10*, 6095-6206.

[7] Rodionova, G.; Lenes, M.; Eriksen, Ø.; Gregersen, Ø. Surface Chemical Modification of Microfibrillated Cellulose: Improvment of Barrier Properties for Packaging Applications. *Cellulose* **2011**, *18*, 127-134.

[8] Hyde, G. K.; McCullen, S. D.; Jeon, S.; Stewart, S. M.; Jeon, H.; Loboa, E. G.; Parsons, G.N. Atomic Layer Deposition and Biocompatibility of Titanium Nitride Nano-Coatings on Cellulose Fiber Substrates. *Biomed. Mater.* **2009**, *4*, 025001.

[9] Glavan, A. C.; Martinez, R. V.; Subramaniam, A. B.; Yoon, H. J.; Nunes, R. M. D.; Lange, H.; Thuo, M. M.; Whitesides, G. M. Omniphobic "R^F Paper" Produced by Silanization of Paper with Fluoroalkyltrichlorosilanes. *Adv. Funct. Mater.* **2014**, *24*, 60-70.

[10] Nyström, D.; Lindqvist, J.; Östmark, E.; Antoni, P.; Carlmark, A.; Hult, A.; Malmström, E. Superhydrophobic and Self-Cleaning Bio-Fiber Surfaces via ATRP and Subsequent Postfunctionalization. *ACS Appl. Mater. Interfaces.* **2009**, *1*, 816-823.

[11] Song, J.; Rojas, O. J. Approaching Super-Hydrophobicity from Cellulosic Materials: A Review. Nord. *Pulp. Pap. Res. J.* **2013**, *28*, 216-238.

[12] George, S. M. Atomic Layer Deposition: An Overview. *ACS Chem. Rev.* **2010**, *110*, 111-131.

[13] Miikkulainen, V.; Leskela, M.; Ritala, M.; Puurunen, R. L. Crystallinity of Inorganic Films Grown by Atomic Layer Deposition: Overview and General Trends. *J. Appl. Phys*. **2013**, *113*, 021301.

[14] Langereis, E.; Creatore, M.; Heil, S. B. S.; Van de Sanden, M. C. M.; Kessels, W. M. M. Plasma-Assisted Atomic Layer Deposition of Moisture Permeation Barriers on Polymers. *Appl. Phys. Lett.* **2006**, *89*, 081915.

[15] Ferguson, J. D.; Weimer, A. W.; George, S. M. Atomic Layer Deposition of Al_2O_3 Films on Polyethylene Particles. *Chem. Mater*. **2004**, *16*, 5602-5609.

[16] Lee, K.; Jur, J. S.; Kim, D. H.; Parsons, G. N. Mechanisms for Hydrophilic/Hydrophobic Wetting Transitions on Cellulose Cotton Fibers Coated Using Al_2O_3 Atomic Layer Deposition. *J. Vac. Sci. Technol. A.* **2012**, *30*, 01A163.

[17] Dameron, A. A.; Davidson, S. D.; Bruton, B. B.; Carcia, P. F.; McLean, R. S.; George, S. M. Gas Diffusion Barriers on Polymers Using Multilayers Fabricated by Al_2O_3 and Rapid SiO_2 Atomic Layer Deposition. *J. Phys. Chem. C.* **2008**, 112, 4573-4580.

[18] Hirvikorpi, T.; Vaha-Nissi, M.; Nikkola, J.; Harlin, A.; Karppinen, M. Thin Al_2O_3 Barrier Coatings onto Temerature-Sensitive Packaging Materials by Atomic Layer Deposition. *Surf. Coat. Technol.* **2011**, *205*, 5088-5092.

[19] Hirvikorpi, T.; Laine, R.; Vaha-Nissi, M.; Kilpi, V.; Salo, E.; Li, W. M.; Lindfors, S.; Vartiainen, J.; Kentta, E.; Nikkola, J.; Harlin, A.; Kostamo, J. Barrier Properties of Plastic Films Coated with and Al_2O_3 Layer by Roll-to-Toll Atomic Layer Deposition. *Thin Solid Films* **2014**, *550*, 164-169.

[20] Meyer, J.; Schmidt, H.; Kowalsky, W.; Riedl, T.; Kahn, A. The Origin of Low Water Vapor Transmission Rates Through Nanolaminate Gas-Diffusion Barriers Grown by Atomic Layer Deposition. *Appl. Phys. Lett*. **2010**, *96*, 243308.

[21] Hirvikorpi, T.; Vaha-Nissi, M.; Mustonen, T.; Iiskola, E.; Karppinen, M. Atomic Layer Deposited Aluminum Oxide Barrier Coatings for Packaging Materials. *Thin Solid Films* **2010**, *518*, 2654-2658.

[22] Hirvikorpi, T.; Vaha-Nissi, M.; Harlin, A.; Marles, J.; Miikkulainen, V.; Karppinen, M. Effect of Corona Pre-treatment on the Performance of Gas Barrier Layers Applied by Atomic Layer Deposition onto Polymer-Coated Paperboard. *Appl. Surf. Sci.* **2010**, *257*, 736-740.

[23] Hyde, G. K.; Park, K.J.; Stewart, S. M.; Hinestroza, J. P.; Parsons, G. N. Atomic Layer Deposition of Conformal Inorganic Nanoscale Coatings on Three-Dimensional Natural Fiber Systems: Effect of Surface Topology on Film Growth Characteristics. *Langmuir* **2007**, *23*, 9844-9849.

[24] Hyde, G. K.; Scarel, G.; Spagnola, J. C.; Peng, Q.; Lee, K.; Gong, B.; Roberts, K. G.; Roth, K. M.; Hanson, C. A.; Devine, C. K.; Stewart, S. M.; Hojo, D.; Na, J. S.; Jur, J. S.; Parsons, G. N. Atomic Layer Deposition and Abrupt Wetting Transitions on Nonwoven Polypropylene and Woven Cotton Fabrics. *Langmuir* **2010**, *26*, 2550-2558.

[25] Edy, R.; Huang, X.; Guo, Y.; Zhang, J.; Shi, J. Influence of Argon Plasma on the Deposition of Al_2O_3 Film onto the PET Surfaces by Atomic Layer Deposition. *Nanoscale Res. Lett*. **2013**, *8*, 1-9.

[26] Massoquete, A; Lavrykov, S. A.; Ramarao, B. V.; Goel, A.; Ramaswamy, S. The Effect of Pulp Refining on Lateral and Transverse Moisture Diffusion in Paper. *TAPPI J.* **2005**, *4*, 3-8.

[27] Nakagaito, A. N.; Yano, H. The Effect of Morphological Changes from Pulp Fiber Towards Nano-Scale Fibrillated Cellulose on the Mechanical Properties of High-Strength Plant Fiber Based Composites. *Appl. Phys. A: Mater. Sci. Process.* **2004**, *78*, 547-552.

[28] Korehei, R.; Jahangiri, P.; Nikbakht, A.; Martinez, M.; Olson, J. Effects of Drying Strategies and Microfibrillated Cellulose Fiber Content on the Properties of Foam-Formed Paper. *J. Wood Chem. Technol.* **2015**, DOI: 10.1080/02773813.2015.1116012.

[29] Gharehkhani, S.; Sadeghinezhad, E.; Kazi, S. N.; Yarmand, H.; Badarudin, A.; Safaei, M. R.; Zubir, M. N. Basic Effects of Pulp Refining on Fiber Properties-A Review. *Carbohydr. Polym*. **2015**, *115*, 785-803.

[30] Missoum, K.; Belgacem, M. N.; Bras, J. Nanofibrillated Cellulose Surface Modification: A Review. *Materials* **2013**, *6*, 1745-1766.

[31] Kietzig, A. M.; Mirvakili, M.; Kamal, S.; Englezos, P.; Hatzikiriakos, S. G. Laser-Patterned Super-Hydrophobic Pure Metallic Substrates: Cassie to Wenzel Wetting Transitions. *J. Adhes. Sci. Technol*. **2011**, *25*, 2789-2809.

[32] Young, T. An Essay on the Cohesion of Fluids. *Phil. Trans. R. Soc. Lond*. **1805**, *95*, 65-87.

[33] Wenzel, R. N. Resistance of Solid Surfaces to Wetting by Water. *Ind. Eng. Chem*. **1936**, *28*, 988-994.

[34] Baxter, S.; Cassie, A. B. D. The Water Repellency of Fabrics and a New Water Repellency Test. *J. Tex. Inst.* **1945,** *36*, 67-90.

[35] Joanny, J. F.; de Gennes, P. G. A Model for Contact Angle Hysteresis. *J. Chem. Phys.* **1984**, *81*, 552-562.

[36] Vander Wielen, L. C. Dielectric Barrier Discharge-Initiated Fiber Modification. *Ph.D. Thesis*, Georgia Institute of Technology, USA, June 2004.

[37] Xie, L.; Tang, Z.; Jiang, L.; Breedveld, V.; Hess, D. W. Creation of Superhydrophobic Wood Surfaces by Plasma Etching and Thin-Film Deposition. *Surf. Coat. Technol.* **2015**, *281*, 125-132.

[38] Langereis, E.; Keijmel, J.; Van de Sanden, M. C. M.; Kessels, W. M. M. Surface Chemistry of Plasma-Assisted Atomic Layer Deposition of Al_2O_3 Studied by Infrared Spectroscopy. *Appl. Phys. Lett.* **2008**, *92*, 231904.

[39] Awada, H.; Elchinger, P. H.; Faugeras, P. A.; Zerrouki, C.; Montplaisir, D.; Broullette, F.; Zerrouki, R. Chemical Modification of Kraft Cellulose Fibers: Influence of Pretreatment on Paper Properties. *BioResources* **2015**, 10, 2044-2056.

[40] Nair, S. S.; Zhu, J. Y.; Deng, Y.; Ragauskas, A. J. High Performance Green Barriers Based on Nanocellulose. *Sustainable Chem. Processes* **2014**, *2*, 1-7.

[41] Findenig, G.; Leimgruber, S.; Kargl, R.; Spirk, S.; Stana-Kleinschek, K.; Ribitsch, V. Creating Water Vapor Barrier Coatings from Hydrophilic Components. *ACS Appl. Mater. Interfaces* **2012**, 4, 3199-3206.

[42] Mirvakili, S. M.; Mirvakili, M.; Englezos, P.; Madden, J. D. W.; Hunter, I. W. High-Performance Supercapacitors from Niobium Nanowire Yarns. *ACS Appl. Mater. Interfaces*. **2015**, 7, 13882-13888

Table of Content/Graphic abstract